Optics Letters

172 fs, 24.3 kW peak power pulse generation from a Ho-doped fiber laser system

Mengmeng Wang,[1,†] Hui Zhang,[2,†] Rongling Wei,[1] Zexiu Zhu,[1] Shuangchen Ruan,[1] Peiguang Yan,[1] Jinzhang Wang,[1,*] Tawfique Hasan,[3] and Zhipei Sun[4,5]

[1]Shenzhen Key Laboratory of Laser Engineering, College of Optoelectronic Engineering, Shenzhen University, Shenzhen 518060, China
[2]Central Laboratory, University of Chinese Academy of Sciences—Shenzhen Hospital, Shenzhen 518106, China
[3]Cambridge Graphene Centre, University of Cambridge, Cambridge CB3 0FA, UK
[4]Department of Electronics and Nanoengineering, Aalto University, Aalto FI-00076, Finland
[5]QTF Centre of Excellence, Department of Applied Physics, Aalto University, Aalto FI-00076, Finland
*Corresponding author: jzwang@szu.edu.cn

Received 3 July 2018; revised 21 July 2018; accepted 21 July 2018; posted 23 July 2018 (Doc. ID 337596); published 19 September 2018

We demonstrate a high-peak-power femtosecond fiber laser system based on single-mode holmium (Ho)-doped fibers. 833 fs, 27.7 MHz pulses at 2083.4 nm generated in a passively mode-locked Ho fiber laser are amplified and compressed to near transform-limited 172 fs, 7.2 nJ pulses with 24.3 kW peak power. We achieve this performance level by using the soliton effect and high-order soliton compression. To the best of our knowledge, this is the first demonstration of sub-200 fs pulses, with peak power exceeding 10 kW from a Ho-doped single-mode fiber laser system without using bulk optics compressors.

OCIS codes: (060.2320) Fiber optics amplifiers and oscillators; (320.7090) Ultrafast lasers; (060.4370) Nonlinear optics, fibers; (060.5530) Pulse propagation and temporal solitons.

https://doi.org/10.1364/OL.43.004619

High-power femtosecond fiber lasers have been widely developed over the past few decades. Their advantages in compact design, simple heat dissipation, high beam quality, and turnkey operation make them attractive over the solid-state lasers. Among them, 2 μm fiber lasers are of great interest because of their widespread use in the plastic materials processing, medical surgery, and gas sensing [1,2]. In particular, ultrafast pulse sources at 2 μm can be efficiently extended to "fingerprint" mid-infrared spectral region through nonlinear frequency conversion [3–5]. Further, these sources are very suitable for efficient generation of XUV/soft x-rays via high-order harmonic generation [6].

Thulium (Tm)-doped fibers are the most common gain media at a 2 μm spectral region in fiber oscillators, due to their broad (~1.7 to 2.1 μm) gain bandwidths. However, this bandwidth usually cannot be fully exploited. For example, the optimal operation spectral range is typically restricted to 1.9–2.0 μm [7–9], which coincides with unwanted water and atmospheric molecular absorption lines [4]. These spectral absorption lines deteriorate the compressed pulse, as well as the beam quality at high average power [10]. These drawbacks can be avoided by shifting the wavelength beyond 2.0 μm. Raman-induced soliton self-frequency shift (SSFS) has been demonstrated generating femtosecond pulses with wavelength tuning ranges up to 2.3 μm [11]. However, compared to the oscillator, SSFS often introduces a larger amplitude and phase noise [12], making their applications unattractive for detection of signals with a small modulation depth. An alternative approach is to use oscillators based on single or co-doping with holmium (Ho) fibers that emit wavelength centered at ~2.05 μm. To this end, there has been significant progress in the development of Ho-doped [13–17] or Tm/Ho [18–21] co-doped ultrafast fiber oscillators. Pulse energy as high as 2.55 nJ has been directly achieved from an all-fiber graphene-mode-locked Ho-doped fiber laser [22]. By using dispersion-managed techniques, 160 fs pulses can be generated in a Ho fiber oscillator [23]. However, the performance of these oscillators is typically limited in terms of pulse energy (<3 nJ), peak power (<10 kW), and average power (few tens of mW). Although they can potentially be directly improved by using fiber amplifiers, the pulse duration is expected to be significantly stretched or distorted if no appropriate dispersion or nonlinearity management is used [17,24].

Chirped pulse amplification (CPA) is a widely accepted strategy that can be used to greatly improve the average power, peak power, and pulse energy, while maintaining the pulse at the femtosecond level. Using a Martinez-type compressor [25] and a chirped volume Bragg grating compressor [26], CPA systems based on Tm/Ho co-doped fibers can produce ~380 fs pulses at 2.08 and 2.05 μm, with pulse energies of 10.2 and 570 nJ, respectively. However, bulk optics is required to compress the pulse, eliminating the flexibility of the fiber output and probably suffering from spatial chirp. Their achievable pulse durations are also restricted by the oscillator spectrum,

as the gain filtering during the amplification would narrow the amplified spectrum and broaden the pulse duration. In contrast, the soliton effect and high-order soliton compression can be exploited during the amplification in gain fibers to significantly shorten the pulse duration and increase the energy without the aid of external bulk compressors [27,28]. Hence, the amplifier system can work with an all-fiber configuration. Indeed, 100 fs pulses with energy as large as 7.4 nJ and peak power as high as 54 kW at 1.5 μm have been directly achieved in a single-stage erbium-doped fiber amplifier without using the CPA [29].

In this Letter, we demonstrate a high-peak-power femtosecond Ho-doped fiber laser system. The fibers used in the system are single mode. The seed pulse is offered by a Ho-doped fiber oscillator delivering 833 fs pulses at 2.08 μm and then amplified in the following Ho-doped fiber amplifier. Due to the soliton effect and high-order soliton compression, our system is able to generate near-transform-limited 172 fs pulses with 24.3 kW peak power, representing, to the best of our knowledge, the highest peak power ever achieved from a single-mode Ho-doped fiber laser system without the use of bulk optics compressors.

The schematic of the experimental setup is depicted in Fig. 1. The system is constructed by a seed oscillator and a single-stage all-fiber amplifier. All of the fibers are single-mode operation, ensuring a high beam quality. Mode-locking operation of the oscillator is driven by the nonlinear polarization evolution, which consists of two $\lambda/4$ waveplates, one $\lambda/2$ waveplate, and a polarization-dependent isolator. All of the waveplates, aspheric lenses, and isolators are assembled in a compact 76 mm × 38.1 mm × 41.1 mm box to improve the mechanical stability and, hence, achieve reliable and turnkey self-starting mode locking. The other components of the oscillator include a 1.3 m long Ho-doped gain fiber (Nufern SM-HDF-10/130) with a 10 μm core diameter, an output coupler (OC) and a 1950/2080 nm wavelength-division multiplexer (WDM). The forward pump light is offered by a homemade Tm-doped fiber laser (TDFL) emitting at 1948 nm with the maximum power up to 2 W. A 20% fraction of intra-cavity light is coupled to the output port. Since the optical nonlinearity of silica fiber decreases at long wavelengths, a 3 m long piece of standard single-mode fiber (SMF-28e) is inserted into the cavity to enhance the nonlinear phase accumulation. This results in an easier initialization of mode locking. The dispersion of the passive fibers and the gain fiber are estimated as −0.105 ps^2/m and −0.112 ps^2/m at 2.08 μm [22], respectively. The total cavity length is ∼7.4 m, and the corresponding net cavity dispersion is estimated as ∼ − 0.78 ps^2 at 2.08 μm.

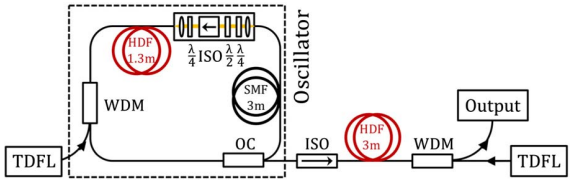

Fig. 1. Schematic of the femtosecond Ho-doped fiber laser system. TDFL, thulium-doped fiber laser; WDM, wavelength-division multiplexer; OC, optical coupler; SMF, single-mode fiber; $\lambda/4$, quarter-wave plate; $\lambda/2$, half-wave plate; ISO, isolator; HDF, holmium-doped fiber.

The fiber amplifier consists of a 3 m long Ho-doped fiber and a WDM, the same types as above. The gain fiber is backward core-pumped by another homemade TDFL with a maximum power up to 2.32 W. An isolator placed between the oscillator and amplifier is used to prevent the residual pump light of TDFL and the back-scattering light of the fiber amplifier from entering into the oscillator to affect the mode-locking operation.

Above a pump power of 560 mW of the oscillator, reliable self-starting mode-locking operation is achieved, with an average power of 9.85 mW and a pulse repetition rate of 27.7 MHz, corresponding to a pulse energy of 0.36 nJ. A frequency-resolved optical gating (FROG) device and an optical spectrum analyzer (OSA, Yokogawa AQ6375) are employed to characterize the output pulse features. The error between the measured and retrieved FROG traces of pulses generated from the oscillator is 0.3%. The retrieved and measured spectra have good agreement, as shown in Fig. 2(a), indicating good reliability of our FROG measurement. The spectrum is centered at 2083.4 nm and has a 3 dB bandwidth of 6.1 nm, with clear sidebands typical for soliton mode-locking operation. Since the Kelly sidebands are generally in the form of a long duration pedestal with low intensity accompanied with the soliton [30], they cannot be efficiently converted to the second harmonic via the BBO crystal of the FROG device. As a result, the retrieved spectrum from FROG shows no clear sidebands [see Fig. 2(a)]. We note a small modulation in the peak of the measured spectrum. This could be caused by the polarization dispersion, as it can be changed by tuning the waveplates. We note that such modulation does not affect the following amplification results. The ratio of the Kelly sidebands to the total energy is ∼19%, as measured by using a diffraction grating following a knife-edge method, is close to the ratio (∼14.5%) calculated by spectral integration in Fig. 2(a). In our experiment, the actual main pulse energy could be slightly higher than 81%, as the pedestal power in the Kelly sidebands still contributes part of the energy to the main pulse. Figure 2(b) depicts the pulse profile retrieved from the FROG trace, with a pulse duration of 833 fs (corresponding to a time bandwidth product of 0.35), close to the Fourier limit if a $sech^2$ pulse is assumed. A small pedestal with respect to the Kelly sidebands could be observed beneath the main pulse. A wide span autocorrelation trace (AC) is carried out to confirm single-pulse operation, as shown in the inset of Fig. 2(b). Both the spectral and temporal phases are close to zero [see Figs. 2(a) and 2(b)], further confirming a relatively low chirp of the pulse.

The pulses generated from the oscillator are then sent to the following amplifier stage. Figures 3(a) and 3(b) depict the

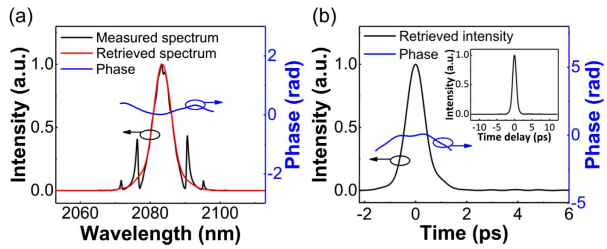

Fig. 2. Characteristics of the oscillator. (a) Measured spectrum (black) from an OSA and retrieved spectrum (red) and phase (blue) from the FROG. (b) Retrieved intensity (black) and phase (blue) in the time domain. Inset, measured AC trace.

evolution of a pulse profile and spectrum as soon as the pump power of the amplifier is increased from 1.65 to 2.32 W, respectively. Initially, the pulse duration monotonically decreases, along with the increase of pump power. After reaching the minimal value of 172 fs at 1.98 W pump power, the pulse duration gradually increases along with the pump power. This can be explained by the soliton effect in combination with the high-order soliton generation [29]. The initial stage of amplification raises the peak power so that a fundamental soliton is formed, where the relationship $\tau_s = 3.52|\beta_2|/(\gamma E_p)$ is satisfied [28]. Here, τ_s is the fundamental soliton duration, β_2 is the group velocity dispersion, γ is the nonlinearity coefficient, and E_p is the pulse energy. As soon as the soliton order reaches $N = 1$, the pulse tries to keep it during the amplification by reducing the pulse duration. However, when the peak power of the soliton is too high to maintain $N = 1$, the pulse evolves into a high-order soliton ($N > 1$), where a shorter pulse width could be obtained under proper pump power. By that time, the spectrum becomes so wide that the gain filtering plays an important role in reducing the spectral width and broadening the pulse. Upon further increase in the pump power, the Raman effect becomes significant, and a separate Raman soliton is formed [see Fig. 3(a)] [28]. Both spectral broadening and narrowing, as well as Raman shifting, are clearly evident in Fig. 3(b). A similar evolution trend could also be observed by altering the gain fiber length with fixed pump power. It should be noted that in order to make the pulse measurement exact, we use a $\lambda/4$ waveplate and a $\lambda/2$ waveplate to convert the output pulse into horizontal polarization, the working polarization of our FROG. The FROG measurement error is below 1.2% in a 64×64 grid size for each measurement, even with a complicated spectrum. We note that <2% error is acceptable as described in the FROG manual.

The total pulse energy increases from 2.8 to 10 nJ when the pump power increases from 1.4 to 2.32 W, as shown in Fig. 3(c). Higher energy is limited by the available pump power of our homemade TDFL. By subtracting the energy of the sidebands (~19% of total energy), the peak powers at different pump powers could be derived from integrating the whole temporal waveform, as shown in Fig. 3(c). The highest peak power is 24.3 kW, where the corresponding pulse width and energy are 172 fs and 7.2 nJ, respectively. The available peak power is limited by the fiber nonlinearity. A larger mode area gain fiber is expected to be capable of supporting a higher peak power [29].

Figure 4 records the output pulse features at the pump power of 1.98 W, where the pulse peak power is highest (24.3 kW). The measured and retrieved spectra have good agreement [see Fig. 4(a)], with the exception of a mismatch at the sidebands and small middle peak, as explained previously. Different slopes of the spectral phase $\varphi(\omega)$ indicate that most of the light at the 2078.4–2089.6 nm range shifts away from the main pulse, as the group delay of a pulse is determined by the spectral phase, $\tau_{gr} = d\varphi(\omega)/d\omega$ [24]. The shifting part is ~18%, estimated by integrating the measured spectrum. This is close to the ratio (~20.8%) of the left side lobe to the entire pulse in Fig. 3(b). Figure 4(b) illustrates the pulse profile, which has a pulse duration of 172 fs, close to the Fourier transform limit of 157 fs. The side lobes of the pulse shape are the inherent nature of high-order soliton compression [28]. The stronger left lobe could be partially enhanced by the negative chirp induced by the SMF-28e pigtail fibers of the isolator and the OC between the oscillator and amplifier. We experimentally find that such enhancement can be reduced by inserting a dispersion compensating fiber (DCF) to dechirp the pulse before sending it to the amplifier. However, the achievable shortest pulse duration becomes >200 fs. This is because unlike chirped pulses, the spectral components in an unchirped pulse are homogeneously distributed and are simultaneously amplified during the amplification. Therefore, it is expected that unchirped pulses will suffer from stronger gain filtering and, thus, have a longer pulse width after amplification than chirped pulses. Therefore, in order to achieve the shortest pulse and highest peak power, we do not use the DCF. By integrating over the whole temporal range, we find that more than 72% energy is located at the main pulse.

The soliton order of the pulse in Fig. 4 can be calculated by $N = (\gamma P_0 \tau^2/|\beta_2|)^{1/2}$ [28]. Here, P_0 is the peak power, τ is the

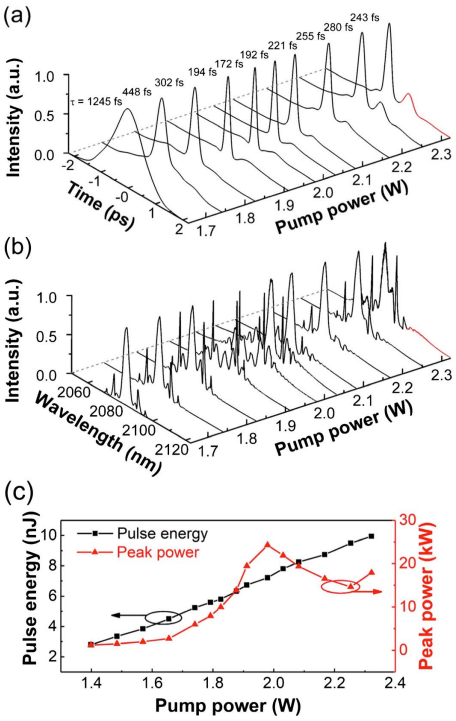

Fig. 3. Evolution of the (a) output pulse profile and (b) spectrum of the amplifier under different pump powers. The red parts depict a Raman shift in time and spectral domain. (c) Pulse energy and peak power of the amplifier versus pump power.

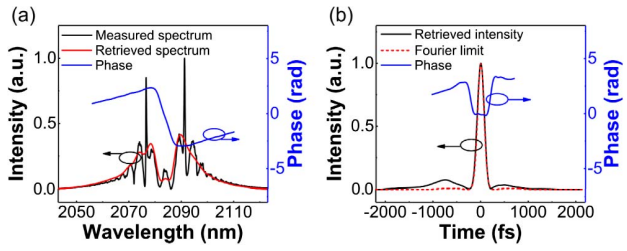

Fig. 4. Characteristics of the output pulses at the pump power of 1.98 W. (a) Measured spectrum (black) from an OSA and retrieved spectrum (red) and phase (blue) from the FROG. (b) Retrieved intensity (black) and phase (blue) in the time domain and calculated Fourier-limit pulse.

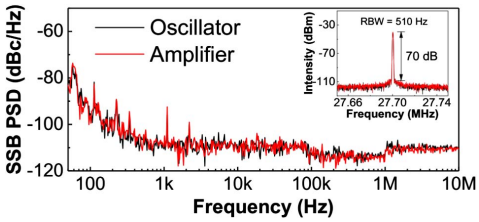

Fig. 5. SSB PSD (50 Hz to 10 MHz) of the first harmonic of the oscillator and amplifier. Inset, RF spectrum of the oscillator and amplifier with a resolution bandwidth (RBW) of 510 Hz.

pulse width, β_2 is the fiber group velocity dispersion, and γ is the fiber nonlinearity which is calculated to be 0.61 $W^{-1} \cdot km^{-1}$ at 2.08 μm in an SMF-28e fiber. This gives a soliton order of ~2.05, confirming high-order soliton compression. We also use an SMF-28e fiber to check the high-order soliton. However, although the spectrum evolution with fiber length is clear, we are unable to recompress the pulse due to the Raman scattering.

To further check the stability of the higher-order soliton, we use a radio frequency (RF) spectrum analyzer (Keysight, N9010B) to characterize the noise. Figure 5 shows the single-sideband (SSB) power spectral density (PSD) from 50 Hz to 10 MHz of the first harmonic of the oscillator and amplifier. No significant difference is observed between them, indicating that the high-order soliton generation almost does not induce extra noise. The RF spectra also show no difference and have a signal-to-noise higher than 70 dB [see the inset of Fig. 5]. The sharp noise spikes below 1 kHz mainly arise from the acoustics and environmental vibrations. It should be noted that due to the limitation of the noise floor of our instrument, we are unable to record the noise below −110 dBc/Hz. However, our spectrum analyzer still could be used to qualitatively characterize the noise change between the oscillator and amplifier.

In summary, we have demonstrated a high-peak-power femtosecond Ho-doped single-mode fiber laser system that produces pulses with 172 fs duration, 24.3 kW peak power, and 7.2 nJ energy at 2.08 μm. Compared to the traditional CPA technique, our system does not require external bulk optics to compress the pulses. The soliton effect and high-order soliton compression in the amplifier play a major role in shortening the pulse width and increasing the energy, enabling truly single-mode fiber output and, therefore, a high beam quality. The pulse duration and the pulse energy have ~5-fold and ~20-fold improvements, respectively, compared to the oscillator. Such a compact, robust laser system is very attractive for applications in pump-probe experiments, mid-IR generation, and remote gas sensing.

Funding. National Key RD Program of China (2016YFA0401100); National Natural Science Foundation of China (NSFC) (61504086, 61605122, 61775146); Natural Science Foundation of Guangdong Province (2016A030310049); Shenzhen Science and Technology Program (JCYJ20160427105041864, JCYJ20160428174445840, JSGG20150512162504354, KQJSCX20160226194031); Engineering and Physical Sciences Research Council (EPSRC) (EP/L016087/1); Seventh Framework Programme (FP7) (631610); Academy of Finland (276376, 284548, 295777, 304666, 312297, 312551, 314810); Tekes (OPEC).

†These authors contributed equally to this Letter.

REFERENCES

1. M. E. Fermann and I. Hartl, IEEE J. Sel. Top. Quantum Electron. **15**, 191 (2009).
2. K. Scholle, S. Lamrini, P. Koopmann, and P. Fuhrberg, *2 μm Laser Sources and Their Possible Applications* (2010).
3. G. Imeshev, M. E. Fermann, K. L. Vodopyanov, M. M. Fejer, X. Yu, J. S. Harris, D. Bliss, and C. Lynch, Opt. Express **14**, 4439 (2006).
4. A. Schliesser, N. Picqué, and T. W. Hänsch, Nat. Photonics **6**, 440 (2012).
5. N. Leindecker, A. Marandi, R. L. Byer, K. L. Vodopyanov, J. Jiang, I. Hartl, M. Fermann, and P. G. Schunemann, Opt. Express **20**, 7046 (2012).
6. M. Gebhardt, C. Gaida, F. Stutzki, S. Hädrich, C. Jauregui, J. Limpert, and A. Tünnermann, Opt. Lett. **42**, 747 (2017).
7. M. Zhang, E. J. R. Kelleher, F. Torrisi, Z. Sun, T. Hasan, D. Popa, F. Wang, A. C. Ferrari, S. V. Popov, and J. R. Taylor, Opt. Express **20**, 25077 (2012).
8. J. Wang, X. Liang, G. Hu, Z. Zheng, S. Lin, D. Ouyang, X. Wu, P. Yan, S. Ruan, Z. Sun, and T. Hasan, Sci. Rep. **6**, 28885 (2016).
9. M. Chernysheva, A. Bednyakova, M. Al Araimi, R. C. T. Howe, G. Hu, T. Hasan, A. Gambetta, G. Galzerano, M. Rümmeli, and A. Rozhin, Sci. Rep. **7**, 44314 (2017).
10. M. Gebhardt, C. Gaida, F. Stutzki, S. Hädrich, C. Jauregui, J. Limpert, and A. Tünnermann, Opt. Express **23**, 13776 (2015).
11. J. Wang, S. Lin, X. Liang, M. Wang, P. Yan, G. Hu, T. Albrow-Owen, S. Ruan, Z. Sun, and T. Hasan, Opt. Lett. **42**, 3518 (2017).
12. U. Keller, K. D. Li, M. J. W. Rodwell, and D. M. Bloom, IEEE J. Quantum Electron. **25**, 280 (1989).
13. A. Chamorovskiy, A. V. Marakulin, S. Ranta, M. Tavast, J. Rautiainen, T. Leinonen, A. S. Kurkov, and O. G. Okhotnikov, Opt. Lett. **37**, 1448 (2012).
14. A. Y. Chamorovskiy, A. V. Marakulin, A. S. Kurkov, and O. G. Okhotnikov, Laser Phys. Lett. **9**, 602 (2012).
15. J. Sotor, M. Pawliszewska, G. Sobon, P. Kaczmarek, A. Przewolka, I. Pasternak, J. Cajzl, P. Peterka, P. Honzátko, and I. Kašík, Opt. Lett. **41**, 2592 (2016).
16. P. Li, A. Ruehl, C. Bransley, and I. Hartl, Laser Phys. Lett. **13**, 065104 (2016).
17. M. Hinkelmann, D. Wandt, U. Morgner, J. Neumann, and D. Kracht, Opt. Express **25**, 20522 (2017).
18. S. Kivisto, T. Hakulinen, M. Guina, and O. G. Okhotnikov, IEEE Photon. Technol. Lett. **19**, 934 (2007).
19. Q. Wang, J. Geng, Z. Jiang, T. Luo, and S. Jiang, IEEE Photon. Technol. Lett. **23**, 682 (2011).
20. R. Kadel and B. R. Washburn, Appl. Opt. **51**, 6465 (2012).
21. X. Jin, X. Wang, X. Wang, and P. Zhou, Appl. Opt. **54**, 8260 (2015).
22. M. Pawliszewska, T. Martynkien, A. Przewłoka, and J. Sotor, Opt. Lett. **43**, 38 (2018).
23. P. Li, A. Ruehl, U. Grosse-Wortmann, and I. Hartl, Opt. Lett. **39**, 6859 (2014).
24. G. Agrawal, *Nonlinear Fiber Optics* (Academic, 2012).
25. H. Hoogland, S. Wittek, W. Hänsel, S. Stark, and R. Holzwarth, Opt. Lett. **39**, 6735 (2014).
26. H. Hoogland and R. Holzwarth, Opt Lett. **40**, 3520 (2015).
27. J. Takayanagi, N. Nishizawa, H. Nagai, M. Yoshida, and T. Goto, IEEE Photon. Technol. Lett. **17**, 37 (2005).
28. G. P. Agrawal, *Applications of Nonlinear Fiber Optics* (Academic, 2008).
29. A. Shirakawa, J. Ota, M. Musha, K. I. Nakagawa, K.-I. Ueda, J. R. Folkenberg, and J. Broeng, Opt. Express **13**, 1221 (2005).
30. C. Wan, T. R. Schibli, P. Li, C. Bevilacqua, A. Ruehl, and I. Hartl, Opt. Lett. **42**, 5266 (2017).